EUROPEAN ORGANIZATION FOR NUCLEAR RESEARCH

CERN–EP/2000-094

13 July 2000

Determination of the $e^+e^- \to \gamma\gamma(\gamma)$ cross-section at centre-of-mass energies ranging from 189 GeV to 202 GeV

DELPHI Collaboration

Abstract

A test of the QED process $e^+e^- \to \gamma\gamma(\gamma)$ is reported. The data analysed were collected with the DELPHI detector in 1998 and 1999 at the highest energies achieved at LEP, reaching 202 GeV in the centre-of-mass. The total integrated luminosity amounts to 375.7 pb^{-1}. The differential and total cross-sections for the process $e^+e^- \to \gamma\gamma$ were measured, and found to be in agreement with the QED prediction. 95% Confidence Level (C.L.) lower limits on the QED cut-off parameters of $\Lambda_+ > 330$ GeV and $\Lambda_- > 320$ GeV were derived. A 95% C.L. lower bound on the mass of an excited electron of 311 $\mathrm{GeV/c^2}$ (for λ_γ =1) was obtained. s-channel virtual graviton exchange was searched for, resulting in 95% C.L. lower limits on the string mass scale, $\mathrm{M_S}$: $\mathrm{M_S} > 713\,\mathrm{GeV/c^2}$ ($\lambda = 1$) and $\mathrm{M_S} > 691\,\mathrm{GeV/c^2}$ ($\lambda = -1$).

(Submitted to Physics Letters B)

P.Abreu[22], W.Adam[52], T.Adye[38], P.Adzic[12], Z.Albrecht[18], T.Alderweireld[2], G.D.Alekseev[17], R.Alemany[51], T.Allmendinger[18], P.P.Allport[23], S.Almehed[25], U.Amaldi[29], N.Amapane[47], S.Amato[49], E.G.Anassontzis[3], P.Andersson[46], A.Andreazza[28], S.Andringa[22], P.Antilogus[26], W-D.Apel[18], Y.Arnoud[15], B.Åsman[46], J-E.Augustin[24], A.Augustinus[9], P.Baillon[9], A.Ballestrero[47], P.Bambade[9,20], F.Barao[22], G.Barbiellini[48], R.Barbier[26], D.Y.Bardin[17], G.Barker[18], A.Baroncelli[40], M.Battaglia[16], M.Baubillier[24], K-H.Becks[54], M.Begalli[6], A.Behrmann[54], P.Beilliere[8], Yu.Belokopytov[9], K.Belous[44], N.C.Benekos[33], A.C.Benvenuti[5], C.Berat[15], M.Berggren[24], L.Berntzon[46], D.Bertrand[2], M.Besancon[41], M.S.Bilenky[17], M-A.Bizouard[20], D.Bloch[10], H.M.Blom[32], M.Bonesini[29], M.Boonekamp[41], P.S.L.Booth[23], G.Borisov[20], C.Bosio[43], O.Botner[50], E.Boudinov[32], B.Bouquet[20], C.Bourdarios[20], T.J.V.Bowcock[23], I.Boyko[17], I.Bozovic[12], M.Bozzo[14], M.Bracko[45], P.Branchini[40], R.A.Brenner[50], P.Bruckman[9], J-M.Brunet[8], L.Bugge[34], T.Buran[34], B.Buschbeck[52], P.Buschmann[54], S.Cabrera[51], M.Caccia[28], M.Calvi[29], T.Camporesi[9], V.Canale[39], F.Carena[9], L.Carroll[23], M.V.Castillo Gimenez[51], A.Cattai[9], F.R.Cavallo[5], M.Chapkin[44], Ph.Charpentier[9], P.Checchia[37], G.A.Chelkov[17], R.Chierici[47], P.Chliapnikov[9,44], P.Chochula[7], V.Chorowicz[26], J.Chudoba[31], K.Cieslik[19], P.Collins[9], R.Contri[14], E.Cortina[51], G.Cosme[20], F.Cossutti[9], M.Costa[51], H.B.Crawley[1], D.Crennell[38], G.Crosetti[14], J.Cuevas Maestro[35], S.Czellar[16], J.D'Hondt[2], J.Dalmau[46], M.Davenport[9], W.Da Silva[24], G.Della Ricca[48], P.Delpierre[27], N.Demaria[47], A.De Angelis[48], W.De Boer[18], C.De Clercq[2], B.De Lotto[48], A.De Min[9], L.De Paula[49], H.Dijkstra[9], L.Di Ciaccio[39], J.Dolbeau[8], K.Doroba[53], M.Dracos[10], J.Drees[54], M.Dris[33], G.Eigen[4], T.Ekelof[50], M.Ellert[50], M.Elsing[9], J-P.Engel[10], M.Espirito Santo[9], G.Fanourakis[12], D.Fassouliotis[12], M.Feindt[18], J.Fernandez[42], A.Ferrer[51], E.Ferrer-Ribas[20], F.Ferro[14], A.Firestone[1], U.Flagmeyer[54], H.Foeth[9], E.Fokitis[33], F.Fontanelli[14], B.Franek[38], A.G.Frodesen[4], R.Fruhwirth[52], F.Fulda-Quenzer[20], J.Fuster[51], A.Galloni[23], D.Gamba[47], S.Gamblin[20], M.Gandelman[49], C.Garcia[51], C.Gaspar[9], M.Gaspar[49], U.Gasparini[37], Ph.Gavillet[9], E.N.Gazis[33], D.Gele[10], T.Geralis[12], N.Ghodbane[26], I.Gil[51], F.Glege[54], R.Gokieli[9,53], B.Golob[9,45], G.Gomez-Ceballos[42], P.Goncalves[22], I.Gonzalez Caballero[42], G.Gopal[38], L.Gorn[1], Yu.Gouz[44], V.Gracco[14], J.Grahl[1], E.Graziani[40], P.Gris[41], G.Grosdidier[20], K.Grzelak[53], J.Guy[38], C.Haag[18], F.Hahn[9], S.Hahn[54], S.Haider[9], Z.Hajduk[19], A.Hallgren[50], K.Hamacher[54], J.Hansen[34], F.J.Harris[36], F.Hauler[18], V.Hedberg[9,25], S.Heising[18], J.J.Hernandez[51], P.Herquet[2], H.Herr[9], E.Higon[51], S-O.Holmgren[46], P.J.Holt[36], S.Hoorelbeke[2], M.Houlden[23], J.Hrubec[52], M.Huber[18], G.J.Hughes[23], K.Hultqvist[9,46], J.N.Jackson[23], R.Jacobsson[9], P.Jalocha[19], R.Janik[7], Ch.Jarlskog[25], G.Jarlskog[25], P.Jarry[41], B.Jean-Marie[20], D.Jeans[36], E.K.Johansson[46], P.Jonsson[26], C.Joram[9], P.Juillot[10], L.Jungermann[18], F.Kapusta[24], K.Karafasoulis[12], S.Katsanevas[26], E.C.Katsoufis[33], R.Keranen[18], G.Kernel[45], B.P.Kersevan[45], Yu.Khokhlov[44], B.A.Khomenko[17], N.N.Khovanski[17], A.Kiiskinen[16], B.King[23], A.Kinvig[23], N.J.Kjaer[9], O.Klapp[54], P.Kluit[32], P.Kokkinias[12], V.Kostioukhine[44], C.Kourkoumelis[3], O.Kouznetsov[17], M.Krammer[52], E.Kriznic[45], Z.Krumstein[17], P.Kubinec[7], W.Kucewicz[19], J.Kurowska[53], K.Kurvinen[16], J.W.Lamsa[1], D.W.Lane[1], V.Lapin[44], J-P.Laugier[41], R.Lauhakangas[16], G.Leder[52], F.Ledroit[15], L.Leinonen[46], A.Leisos[12], R.Leitner[31], J.Lemonne[2], G.Lenzen[54], V.Lepeltier[20], M.Lethuillier[26], J.Libby[36], W.Liebig[54], D.Liko[9], A.Lipniacka[46], I.Lippi[37], B.Loerstad[25], J.G.Loken[36], J.H.Lopes[49], J.M.Lopez[42], R.Lopez-Fernandez[15], D.Loukas[12], P.Lutz[41], L.Lyons[36], J.MacNaughton[52], J.R.Mahon[6], A.Maio[22], A.Malek[54], S.Maltezos[33], V.Malychev[17], F.Mandl[52], J.Marco[42], R.Marco[42], B.Marechal[49], M.Margoni[37], J-C.Marin[9], C.Mariotti[9], A.Markou[12], C.Martinez-Rivero[9], S.Marti i Garcia[9], J.Masik[13], N.Mastroyiannopoulos[12], F.Matorras[42], C.Matteuzzi[29], G.Matthiae[39], F.Mazzucato[37], M.Mazzucato[37], M.Mc Cubbin[23], R.Mc Kay[1], R.Mc Nulty[23], G.Mc Pherson[23], E.Merle[15], C.Meroni[28], W.T.Meyer[1], A.Miagkov[44], E.Migliore[9], L.Mirabito[26], W.A.Mitaroff[52], U.Mjoernmark[25], T.Moa[46], M.Moch[18], R.Moeller[30], K.Moenig[9,11], M.R.Monge[14], D.Moraes[49], P.Morettini[14], G.Morton[36], U.Mueller[54], K.Muenich[54], M.Mulders[32], C.Mulet-Marquis[15], L.M.Mundim[6], R.Muresan[25], W.J.Murray[38], B.Muryn[19], G.Myatt[36], T.Myklebust[34], F.Naraghi[15], M.Nassiakou[12], F.L.Navarria[5], K.Nawrocki[53], P.Negri[29], N.Neufeld[52], R.Nicolaidou[41], B.S.Nielsen[30], P.Niezurawski[53], M.Nikolenko[10,17], V.Nomokonov[16], A.Nygren[25], A.Oblakowska Mucha[19], V.Obraztsov[44], A.G.Olshevski[17], A.Onofre[22], R.Orava[16], G.Orazi[10], K.Osterberg[9], A.Ouraou[41], A.Oyanguren[51], M.Paganoni[29], S.Paiano[5], R.Pain[24], R.Paiva[22], J.Palacios[36], Th.D.Papadopoulou[33], L.Pape[9], C.Parkes[9], F.Parodi[14], U.Parzefall[23], A.Passeri[40], O.Passon[54], T.Pavel[25], M.Pegoraro[37], L.Peralta[22], M.Pernicka[52], A.Perrotta[5], C.Petridou[48], A.Petrolini[14], H.T.Phillips[38], F.Pierre[41], M.Pimenta[22], E.Piotto[28], T.Podobnik[45], V.Poireau[41], M.E.Pol[6], G.Polok[19], P.Poropat[48], V.Pozdniakov[17], P.Privitera[39], N.Pukhaeva[17], A.Pullia[29], D.Radojicic[36], S.Ragazzi[29], H.Rahmani[33], J.Rames[13], P.N.Ratoff[21], A.L.Read[34], P.Rebecchi[9], N.G.Redaelli[29], M.Regler[52], J.Rehn[18], D.Reid[32], P.Reinertsen[4], R.Reinhardt[54], P.B.Renton[36], L.K.Resvanis[3], F.Richard[20], J.Ridky[13], G.Rinaudo[47], I.Ripp-Baudot[10], A.Romero[47], P.Ronchese[37], E.I.Rosenberg[1], P.Rosinsky[7], P.Roudeau[20], T.Rovelli[5], V.Ruhlmann-Kleider[41], A.Ruiz[42], H.Saarikko[16], Y.Sacquin[41], A.Sadovsky[17], G.Sajot[15], J.Salt[51], D.Sampsonidis[12], M.Sannino[14], A.Savoy-Navarro[24], Ph.Schwemling[24], B.Schwering[54], U.Schwickerath[18], F.Scuri[48], P.Seager[21], Y.Sedykh[17], A.M.Segar[36], N.Seibert[18], R.Sekulin[38], G.Sette[14], R.C.Shellard[6], M.Siebel[54], L.Simard[41], F.Simonetto[37], A.N.Sisakian[17], G.Smadja[26], O.Smirnova[25], G.R.Smith[38], O.Solovianov[44], A.Sopczak[18], R.Sosnowski[53], T.Spassov[9], E.Spiriti[40], S.Squarcia[14], C.Stanescu[40], M.Stanitzki[18], K.Stevenson[36], A.Stocchi[20], J.Strauss[52], R.Strub[10], B.Stugu[4], M.Szczekowski[53], M.Szeptycka[53], T.Tabarelli[29], A.Taffard[23], F.Tegenfeldt[50], F.Terranova[29], J.Timmermans[32], N.Tinti[5], L.G.Tkatchev[17], M.Tobin[23], S.Todorova[9], B.Tome[22], A.Tonazzo[9], L.Tortora[40], P.Tortosa[51], G.Transtromer[25], D.Treille[9], G.Tristram[8], M.Trochimczuk[53], C.Troncon[28], M-L.Turluer[41], I.A.Tyapkin[17], P.Tyapkin[25], S.Tzamarias[12], O.Ullaland[9], V.Uvarov[44], G.Valenti[9,5], E.Vallazza[48],

P.Van Dam[32], W.Van den Boeck[2], J.Van Eldik[9,32], A.Van Lysebetten[2], N.van Remortel[2], I.Van Vulpen[32], G.Vegni[28], L.Ventura[37], W.Venus[38,9], F.Verbeure[2], P.Verdier[26], M.Verlato[37], L.S.Vertogradov[17], V.Verzi[28], D.Vilanova[41], L.Vitale[48], E.Vlasov[44], A.S.Vodopyanov[17], G.Voulgaris[3], V.Vrba[13], H.Wahlen[54], A.J.Washbrook[23], C.Weiser[9], D.Wicke[9], J.H.Wickens[2], G.R.Wilkinson[36], M.Winter[10], G.Wolf[9], J.Yi[1], O.Yushchenko[44], A.Zalewska[19], P.Zalewski[53], D.Zavrtanik[45], E.Zevgolatakos[12], N.I.Zimin[17,25], A.Zintchenko[17], Ph.Zoller[10], G.Zumerle[37], M.Zupan[12]

[1]Department of Physics and Astronomy, Iowa State University, Ames IA 50011-3160, USA
[2]Physics Department, Univ. Instelling Antwerpen, Universiteitsplein 1, B-2610 Antwerpen, Belgium
and IIHE, ULB-VUB, Pleinlaan 2, B-1050 Brussels, Belgium
and Faculté des Sciences, Univ. de l'Etat Mons, Av. Maistriau 19, B-7000 Mons, Belgium
[3]Physics Laboratory, University of Athens, Solonos Str. 104, GR-10680 Athens, Greece
[4]Department of Physics, University of Bergen, Allégaten 55, NO-5007 Bergen, Norway
[5]Dipartimento di Fisica, Università di Bologna and INFN, Via Irnerio 46, IT-40126 Bologna, Italy
[6]Centro Brasileiro de Pesquisas Físicas, rua Xavier Sigaud 150, BR-22290 Rio de Janeiro, Brazil
and Depto. de Física, Pont. Univ. Católica, C.P. 38071 BR-22453 Rio de Janeiro, Brazil
and Inst. de Física, Univ. Estadual do Rio de Janeiro, rua São Francisco Xavier 524, Rio de Janeiro, Brazil
[7]Comenius University, Faculty of Mathematics and Physics, Mlynska Dolina, SK-84215 Bratislava, Slovakia
[8]Collège de France, Lab. de Physique Corpusculaire, IN2P3-CNRS, FR-75231 Paris Cedex 05, France
[9]CERN, CH-1211 Geneva 23, Switzerland
[10]Institut de Recherches Subatomiques, IN2P3 - CNRS/ULP - BP20, FR-67037 Strasbourg Cedex, France
[11]Now at DESY-Zeuthen, Platanenallee 6, D-15735 Zeuthen, Germany
[12]Institute of Nuclear Physics, N.C.S.R. Demokritos, P.O. Box 60228, GR-15310 Athens, Greece
[13]FZU, Inst. of Phys. of the C.A.S. High Energy Physics Division, Na Slovance 2, CZ-180 40, Praha 8, Czech Republic
[14]Dipartimento di Fisica, Università di Genova and INFN, Via Dodecaneso 33, IT-16146 Genova, Italy
[15]Institut des Sciences Nucléaires, IN2P3-CNRS, Université de Grenoble 1, FR-38026 Grenoble Cedex, France
[16]Helsinki Institute of Physics, HIP, P.O. Box 9, FI-00014 Helsinki, Finland
[17]Joint Institute for Nuclear Research, Dubna, Head Post Office, P.O. Box 79, RU-101 000 Moscow, Russian Federation
[18]Institut für Experimentelle Kernphysik, Universität Karlsruhe, Postfach 6980, DE-76128 Karlsruhe, Germany
[19]Institute of Nuclear Physics and University of Mining and Metalurgy, Ul. Kawiory 26a, PL-30055 Krakow, Poland
[20]Université de Paris-Sud, Lab. de l'Accélérateur Linéaire, IN2P3-CNRS, Bât. 200, FR-91405 Orsay Cedex, France
[21]School of Physics and Chemistry, University of Lancaster, Lancaster LA1 4YB, UK
[22]LIP, IST, FCUL - Av. Elias Garcia, 14-1^{o}, PT-1000 Lisboa Codex, Portugal
[23]Department of Physics, University of Liverpool, P.O. Box 147, Liverpool L69 3BX, UK
[24]LPNHE, IN2P3-CNRS, Univ. Paris VI et VII, Tour 33 (RdC), 4 place Jussieu, FR-75252 Paris Cedex 05, France
[25]Department of Physics, University of Lund, Sölvegatan 14, SE-223 63 Lund, Sweden
[26]Université Claude Bernard de Lyon, IPNL, IN2P3-CNRS, FR-69622 Villeurbanne Cedex, France
[27]Univ. d'Aix - Marseille II - CPP, IN2P3-CNRS, FR-13288 Marseille Cedex 09, France
[28]Dipartimento di Fisica, Università di Milano and INFN-MILANO, Via Celoria 16, IT-20133 Milan, Italy
[29]Dipartimento di Fisica, Univ. di Milano-Bicocca and INFN-MILANO, Piazza delle Scienze 2, IT-20126 Milan, Italy
[30]Niels Bohr Institute, Blegdamsvej 17, DK-2100 Copenhagen Ø, Denmark
[31]IPNP of MFF, Charles Univ., Areal MFF, V Holesovickach 2, CZ-180 00, Praha 8, Czech Republic
[32]NIKHEF, Postbus 41882, NL-1009 DB Amsterdam, The Netherlands
[33]National Technical University, Physics Department, Zografou Campus, GR-15773 Athens, Greece
[34]Physics Department, University of Oslo, Blindern, NO-1000 Oslo 3, Norway
[35]Dpto. Fisica, Univ. Oviedo, Avda. Calvo Sotelo s/n, ES-33007 Oviedo, Spain
[36]Department of Physics, University of Oxford, Keble Road, Oxford OX1 3RH, UK
[37]Dipartimento di Fisica, Università di Padova and INFN, Via Marzolo 8, IT-35131 Padua, Italy
[38]Rutherford Appleton Laboratory, Chilton, Didcot OX11 OQX, UK
[39]Dipartimento di Fisica, Università di Roma II and INFN, Tor Vergata, IT-00173 Rome, Italy
[40]Dipartimento di Fisica, Università di Roma III and INFN, Via della Vasca Navale 84, IT-00146 Rome, Italy
[41]DAPNIA/Service de Physique des Particules, CEA-Saclay, FR-91191 Gif-sur-Yvette Cedex, France
[42]Instituto de Fisica de Cantabria (CSIC-UC), Avda. los Castros s/n, ES-39006 Santander, Spain
[43]Dipartimento di Fisica, Università degli Studi di Roma La Sapienza, Piazzale Aldo Moro 2, IT-00185 Rome, Italy
[44]Inst. for High Energy Physics, Serpukov P.O. Box 35, Protvino, (Moscow Region), Russian Federation
[45]J. Stefan Institute, Jamova 39, SI-1000 Ljubljana, Slovenia and Laboratory for Astroparticle Physics,
Nova Gorica Polytechnic, Kostanjeviska 16a, SI-5000 Nova Gorica, Slovenia,
and Department of Physics, University of Ljubljana, SI-1000 Ljubljana, Slovenia
[46]Fysikum, Stockholm University, Box 6730, SE-113 85 Stockholm, Sweden
[47]Dipartimento di Fisica Sperimentale, Università di Torino and INFN, Via P. Giuria 1, IT-10125 Turin, Italy
[48]Dipartimento di Fisica, Università di Trieste and INFN, Via A. Valerio 2, IT-34127 Trieste, Italy
and Istituto di Fisica, Università di Udine, IT-33100 Udine, Italy
[49]Univ. Federal do Rio de Janeiro, C.P. 68528 Cidade Univ., Ilha do Fundão BR-21945-970 Rio de Janeiro, Brazil
[50]Department of Radiation Sciences, University of Uppsala, P.O. Box 535, SE-751 21 Uppsala, Sweden
[51]IFIC, Valencia-CSIC, and D.F.A.M.N., U. de Valencia, Avda. Dr. Moliner 50, ES-46100 Burjassot (Valencia), Spain
[52]Institut für Hochenergiephysik, Österr. Akad. d. Wissensch., Nikolsdorfergasse 18, AT-1050 Vienna, Austria
[53]Inst. Nuclear Studies and University of Warsaw, Ul. Hoza 69, PL-00681 Warsaw, Poland
[54]Fachbereich Physik, University of Wuppertal, Postfach 100 127, DE-42097 Wuppertal, Germany

1 Introduction

An analysis of two-photon final states using the high energy data sets collected with the DELPHI detector in 1998 and 1999 is reported. The data analysed were collected at e^+e^- collision energies ranging from 188.6 GeV up to 201.6 GeV, corresponding to a total integrated luminosity of 375.7 pb^{-1}.

Final states with two photons are mainly produced by the standard process $e^+e^- \to \gamma\gamma(\gamma)$. This reaction is an almost pure QED process: at orders above α^2, it is mainly affected by QED corrections, such as soft and hard *bremsstrahlung* and virtual corrections, compared to which the weak corrections due to the exchange of virtual massive gauge bosons are very small [1,2,3]. Therefore, any significant deviation between the measured and the QED cross-section could unambiguously be interpreted as the result of non-standard physics.

The Born cross-section for $e^+e^- \to \gamma\gamma(\gamma)$ is given by

$$\sigma^0_{\rm QED} = {\rm K} \cdot \frac{2\pi\alpha}{\rm s}. \tag{1}$$

K depends on the angular acceptance for the final state photons, α is the electromagnetic coupling constant and s is the centre-of-mass energy squared.

Since $\sigma^0_{\rm QED}$ scales with s^{-1}, the combination of measurements taken at different centre-of-mass energy values is straightforward and data taken at neighbouring values of $\sqrt{s}$ can be combined by applying this scaling function.

Previous DELPHI results concerning the process $e^+e^- \to \gamma\gamma(\gamma)$, using LEPI and LEPII data, can be found in references [4,5]. The most recently published results from the other LEP experiments can be found in references [6,7,8].

2 Data sample and apparatus

The data analysed were taken at e^+e^- collision energies of 188.63 ± 0.04 GeV, 191.6 ± 0.04 GeV, 195.5 ± 0.04 GeV, 199.5 ± 0.04 GeV and 201.6 ± 0.04 GeV [9], corresponding to integrated luminosities of 151.9 ± 0.9 pb^{-1}, 25.1 ± 0.1 pb^{-1}, 76.1 ± 0.4 pb^{-1}, 82.6 ± 0.5 pb^{-1} and 40.1 ± 0.2 pb^{-1} respectively. The luminosity was measured by counting the number of Bhabha events at small polar angles, recorded with DELPHI's luminometer: the Small angle TIle Calorimeter (STIC), made of two modules located at $|z| = 220$ cm from the interaction point and with polar angle coverage between 2° and 10° (170° and 178°).

Photon detection and reconstruction relies on the trigger and energy measurement based on two electromagnetic calorimeters: the High density Projection Chamber (HPC) in the barrel region and the Forward ElectroMagnetic Calorimeter (FEMC) in the end-caps. The HPC is a gas-sampling calorimeter, made of 144 modules, each one with 10 lead layers in Rϕ embedded in a gas mixture. It covers polar angles between 42° and 138°. The FEMC is a lead glass calorimeter, covering the polar angle region $[11°, 35°]$ and its complement with respect to 180°. The barrel DELPHI electromagnetic trigger requires coincidence between scintillator signals and energy deposits in HPC while in the forward region the electromagnetic trigger is given by energy deposits in the FEMC lead-glass counters.

The tracking system allows the rejection of charged particles and the recovery of photons converting inside the detector. The DELPHI barrel tracking system relies on the Vertex Detector (VD), the Inner Detector (ID), the Time Projection Chamber (TPC)

and the Outer Detector (OD). In the endcaps, the tracking system relies also on the VD and the TPC (down to about 20° in polar angle), and on the Forward Chambers A and B (FCA, FCB). The VD plays an important role in the detection of charged particle tracks coming from the interaction point. A more detailed description of the DELPHI detector, of the triggering conditions and of the readout chain can be found in [10].

3 Photon reconstruction and identification

The process $e^+e^- \to \gamma\gamma(\gamma)$ yields not only neutral final states but also final states characterized by the presence of charged particle tracks from photon conversions.

Photons converting inside the tracking system, but after the Vertex Detector, are characterized by charged particle tracks and will be refered to as converted photons. Photons reaching the electromagnetic calorimeters before converting, yielding no reconstructed charged particle tracks, will be refered to as unconverted photons. According to this classification, two different algorithms were applied in the photon reconstruction and identification.

The main contamination to $e^+e^- \to \gamma\gamma(\gamma)$ final states comes from radiative Bhabha ($e^+e^- \to e^+e^-(\gamma)$) events with one non-reconstructed electron and the other electron lost in the beam pipe, and from Compton ($e^\pm\gamma$) events. Compton events are produced by the scattering of beam electrons by a quasi-real photon radiated by another incoming electron, resulting mostly in final states with one photon and one electron in the detector, the remaining $e^\pm$ going undetected through the beam-pipe. Both the Bhabha and the Compton backgrounds can however be dramatically reduced if the Vertex Detector is used as a veto for charged particles coming from the interaction point. The event generator used to simulate $e^+e^- \to \gamma\gamma(\gamma)$ was that of Berends and Kleiss [1], while the Bhabha and Compton event generators are BHWIDE and TEEG, described in references [11] and [12] respectively. The generated samples were processed through the full DELPHI simulation and reconstruction chains [10].

3.1 Unconverted photons

Unconverted photon candidates were reconstructed by applying an isolation algorithm to energy deposits in the calorimeters. The algorithm relied on a double cone centered on each energy deposit, with internal and external half angles of 5° and 15° respectively, where the vertices of both cones correspond to the geometric centre of DELPHI. Showers were considered isolated if the total energy inside the double cone was less than 1 GeV. The energy of the isolated neutral particles was re-evaluated as the sum of the energy of all associated deposits inside the inner cone where no charged particles of more than 250 MeV/c were allowed. The direction of the isolated showers was the energy weighted mean of the directions of all associated energy deposits. Such particles, with a total energy above 3 GeV, were identified as photons if the following criteria were fulfilled:

- The polar angle of the energy deposit was inside $[25°, 35°]$, $[42°, 88°]$, $[92°, 138°]$ or $[145°, 155°]$, in order to reduce VD and calorimeter edge effects.
- No VD track element pointed to the direction of the energy deposit within 3° (10°) in azimuthal angle in the barrel (forward) region of DELPHI (a VD track element was defined as at least two hits in different VD layers aligned within an azimuthal angle interval of 0.5°).

- If more than 3 GeV of hadronic energy was associated to a deposit, then at least 90% of it had to be in the first layer of the Hadronic CALorimeter (HCAL).
- For an energy deposit in the HPC, there had to be at least three HPC layers with more than 5% of the total electromagnetic energy, unless the deposit was within 1 degree of the HPC azimuthal intermodular divisions [1].

3.2 Converted photons

Converted photon candidates were reconstructed with the help of a jet clustering algorithm: all particles in the event, with the exception of isolated neutral particles, were forced to be clustered in jets (isolated charged particles were not treated as single particles but as low multiplicity jets). The DURHAM jet algorithm [13] was applied, using as resolution variable $y_{cut} = 0.003$. Low multiplicity jets with less than 6 charged particles were treated as converted photon candidates. These candidates were recovered if they were associated to energy deposits above 3 GeV fulfilling the photon identification criteria described in section 3.1. The requirement that no correlated signals were observed in the VD was a particularly important criterion for the rejection of electrons.

4 Two photon events: $e^+e^- \to \gamma\gamma(\gamma)$

The selected $\gamma\gamma(\gamma)$ sample consisted of events with at least two photons, where at most one was converted. The electromagnetic calorimeters (HPC and FEMC), the TPC and the VD were required to be nominally operational. The analysis was performed in the polar angle interval corresponding to $|\cos\theta^*| \in [0.035, 0.731] \cup [0.819, 0.906]$, where the variable θ^* stands for the polar angle of the photons relative to the direction of the incident electron in the centre-of-mass of the e^+e^- collision[2] after allowing for ISR. The two most energetic photons were required to have energies above 15% of the collision energy and isolation angle of 30° (the isolation angle is the minimum of the angles between the photon and the remaining reconstructed particles in the event). No other particles (with exception of isolated photons) with energy above 3 GeV were allowed in the event. The application of these criteria resulted in an almost pure $\gamma\gamma$ sample, where the contamination from Bhabha and Compton events is about 0.3% and 3% respectively.

The radiation of a third hard photon constrains the two harder photons to be produced at effective $\sqrt{s}$ values which have been tested more accurately using lower energy data. Since the aim of this analysis is to test the QED $e^+e^- \to \gamma\gamma$ reaction at the highest available energies, such final states were not allowed in the selected sample: events with a third hard *bremsstrahlung* photon can be considered as a higher order contribution to $e^+e^- \to \gamma\gamma$ (like the soft *bremsstrahlung* and the virtual contributions), which can be deconvoluted from data by applying a radiative correction factor when evaluating the $e^+e^- \to \gamma\gamma$ Born cross-section. Moreover, the $e^+e^- \to \gamma\gamma\gamma$ contribution can be dramatically reduced if the spatial angle between the two most energetic photons is required to be large. Therefore, a final selection criterion, consisting in requiring that the acollinearity[3] between the two most energetic photons was below 30°, was applied, eliminating most events with a third visible hard photon, and reducing the Compton background to 0.3%. The acollinearity distribution prior to the cut is shown in figure 1(a) for the full data sample, and compared to the $e^+e^- \to \gamma\gamma(\gamma)$ simulation and to the remaining background

[1] The HPC modules are distributed in 6 rings of 24 modules located at $\mathrm{mod}(\phi, 15°) = 7.5°$.

[2] The parameterization of the photon polar angle with θ^* enables the cross-section measurement to be insensitive to photons lost in the beam pipe.

[3] The acollinearity between two directions is the complement to π of the spatial angle between them.

expectations. After imposing all selection criteria, the contamination from Bhabha and Compton events to the selected $\gamma\gamma$ sample was estimated to be 0.6%, and taken into account in the systematic uncertainty.

4.1 $\gamma\gamma$ trigger and selection efficiencies

The trigger efficiency for neutral two-photon final states was computed with Bhabha events using the redundancy of the electromagnetic trigger with the track trigger. It was calculated for each centre-of-mass energy as a function of $|\cos\theta^*|$. The global values obtained for the barrel and endcaps are displayed in table 1.

Final states with one converted photon are triggered by the single track coincidence trigger, whose efficiency is known to be near 100%. Two dedicated samples of Compton ($e^{\pm}\gamma$) events, one with a triggered FEMC photon and another with a triggered HPC photon, were used to cross-check the track trigger efficiency in the barrel and endcaps. The global efficiency for triggering events with one converted photon was confirmed to be above 99% in both regions of the detector, for all data sets, and the resulting uncertainty was taken into account in the global systematic uncertainty.

The selection efficiency for the two-photon event sample was evaluated as a function of $|\cos\theta^*|$ using events from the $e^+e^- \to \gamma\gamma(\gamma)$ generator of Berends and Kleiss [1] passed through the full DELPHI simulation and reconstruction chains [10]. The effect of the calorimeter requirements on the selection efficiency obtained from simulation was cross-checked using a sample of e^+e^- events. These events were selected using information coming exclusively from the tracking detectors. The efficiency was defined as the ratio between the number of events in the subsample of e^+e^- final states fulfilling the calorimetric selection and the total number of selected e^+e^- events. This efficiency was computed as a function of $|\cos\theta^*|$ for both real and simulated Bhabha events. The difference observed between the efficiency for the data and for the simulation was taken as a systematic uncertainty in the $e^+e^- \to \gamma\gamma(\gamma)$ selection efficiency determination.

The global values for the selection efficiency, both in the barrel and in the forward region of DELPHI, are displayed in table 2 along with their statistical and systematic uncertainties. A change in the forward DELPHI particle reconstruction algorithms resulted in a better performance for $\gamma\gamma$ final states for the 1999 data processing compared with that of 1998. However, there was an increase of the systematic uncertainty in the $\gamma\gamma$ selection efficiency.

4.2 $e^+e^- \to \gamma\gamma$ cross-section

The retained $|\cos\theta^*|$ acceptance was divided into 8 bins: the barrel part of the detector, corresponding to $|\cos\theta^*| \in [0.035, 0.731]$ with 7 bins, (each covering $|\Delta\cos\theta^*| = 0.101$, except for the last bin, for which $|\Delta\cos\theta^*| = 0.09$) and the forward region with one bin, $|\cos\theta^*| \in [0.819, 0.906]$. The number of events found in data for each centre-of-mass energy and the expected contribution from the QED process $e^+e^- \to \gamma\gamma(\gamma)$ (corrected for trigger efficiency) are displayed in table 3 as a function of $|\cos\theta^*|$.

The Born cross-section for the reaction $e^+e^- \to \gamma\gamma(\gamma)$ was evaluated through expression (2) for each centre-of-mass energy value,

$$\sigma^0_{\rm dat} = \frac{\mathrm{N}^{\gamma\gamma}}{\mathcal{L}\varepsilon\mathrm{R}} \ \ [\mathrm{pb}]. \tag{2}$$

$\mathrm{N}^{\gamma\gamma}$ is the number of selected events after background subtraction, $\mathcal{L}$ is the integrated luminosity, ε is the product of the selection and trigger efficiencies and R is a radiative

correction factor. The radiative correction factor was evaluated using the Monte Carlo generator of [1]. It was taken as the ratio between the $e^+e^- \to \gamma\gamma(\gamma)$ cross-section computed up to order α^3 to the Born cross-section ($\mathcal{O}(\alpha^2)$) and found to be of the order of 1.07 (1.04) for high (low) photon scattering angles.

A combined value of the Born cross-section at an average centre-of-mass energy of 193.8 GeV, corresponding to a total integrated luminosity of 375.7 pb^{-1}, was obtained through expression (2). The average value of the centre-of-mass energy is obtained weighting the integrated luminosities of the different samples by the corresponding s^{-1} factor.

$N^{\gamma\gamma}$ is taken as the total number of selected events in the five data samples. The average trigger and selection efficiencies were obtained by weighting the global trigger and selection efficiencies of each data set by the corresponding integrated luminosities. The measured Born cross-section for each of the five centre-of-mass energies and the combined result are compared to the QED predictions in table 4 and in the upper right corner of figure 2. The χ^2 of the measured values for the cross-section for the different centre-of-mass energies with respect to the QED prediction was 5.5 with 5 degrees of freedom.

The Born cross-section values for the five centre-of-mass energies measured in the region $0.035 < |\cos\theta^*| < 0.731$, were corrected to the full barrel acceptance of DELPHI, $0.000 < |\cos\theta^*| < 0.742$, and the obtained values are presented in table 4. These are also displayed in figure 2 as a function of the centre-of-mass energy, along with the previously published results, which include LEP I data collected between 1990 and 1992 [4] and former LEP II data collected between 1995 and 1997 [5].

The total systematic errors were obtained by adding in quadrature the uncertainties on the selection efficiency, trigger efficiencies, residual background, luminosity determination and on the radiative corrections (amounting to $\pm 0.5\%$). The systematic uncertainty in the selection efficiency determination is the dominant contribution to the systematic error; with a typical value of $\pm 2.5\%$. This uncertainty reflects residual differences between the real detector response and the simulated one. It is due to effects that cannot be fully described by the detector simulation such as detector instabilities and edge effects of calorimeters. The uncertainty in the luminosity determination was $\pm 0.56\%$. It was obtained by adding in quadrature the $\pm 0.5\%$ systematic uncertainty in the luminosity measurement and the $\pm 0.25\%$ theoretical error in the Bhabha cross-section determination [14].

The $e^+e^- \to \gamma\gamma$ differential Born cross-section was computed as:

$$\frac{\mathrm{d}\sigma^0_{\mathrm{i}}}{\mathrm{d}\Omega} = \frac{\sigma^0_{\mathrm{i}}}{2\pi\Delta\cos\theta^*_{\mathrm{i}}} \ \ [\mathrm{pb/str}], \tag{3}$$

where σ^0_{i} stands for the measured Born cross-section in each $|\cos\theta^*_{\mathrm{i}}|$ interval, (i).

The differential cross-section was computed for each centre-of-mass energy, taking into account the $|\cos\theta^*|$ dependence of trigger and selection efficiencies, radiative corrections and their respective uncertainties. Comparisons between the measured and predicted Born differential cross-sections for each centre-of-mass energy are shown in figure 3. The deficit of $\gamma\gamma$ events for $|\cos\theta^*|$ between 0.237 and 0.338 for $\sqrt{s}$=195.5 GeV was concluded to be a statistical fluctuation: the trigger efficiency for this region was estimated to be about 98% and the counting of energy deposits associated to Bhabha electrons in the same $|\cos\theta^*|$ region showed a good agreement with the simulation expectations.

The differential cross-section extracted from the combined data sets (corresponding to $\sqrt{s_{eff}} = 193.8$ GeV), is compared to the QED prediction in table 5 and in figure 4. The

χ^2 of the differential cross-section binned distribution at the mean centre-of-mass energy with respect to the QED prediction was 3.6 with 8 degrees of freedom.

4.3 Deviations from QED

Possible deviations from QED are described in the context of several models, which express the Born differential cross-section for $e^+e^- \to \gamma\gamma$ as the sum of the QED term and of a deviation term:

$$\frac{\mathrm{d}\sigma^0}{\mathrm{d}\Omega} = \frac{\alpha^2}{\mathrm{s}} \frac{1+\cos^2\theta^*}{1-\cos^2\theta^*} + \left(\frac{\mathrm{d}\sigma}{\mathrm{d}\Omega}\right)^{\mathrm{D}} \quad . \tag{4}$$

Among the models predicting deviations from QED are those described in table 6. The most general parameterization consists of introducing a cut-off parameter in the electron propagators (Λ), reflecting the energy scale up to which the eγ interaction can be described as point-like [15,16].

Deviations from QED could also follow from the t-channel exchange of an excited electron, which, in composite models [17], is parameterized as a function of $\lambda_\gamma/\mathrm{M}^2_{\mathrm{e}^*}$ (the ratio between the coupling of the excited electron to the photon and to the electron and the excited electron mass) and of a kinematic factor, $\mathrm{H}(\cos^2\theta^*)$,

$$\mathrm{H}(\cos^2\theta^*) = \frac{2\mathrm{M}^2_{\mathrm{e}^*}}{\mathrm{s}} \cdot \left(\frac{2\mathrm{M}^2_{\mathrm{e}^*}}{\mathrm{s}} + \frac{1-\cos^2\theta^*}{1+\cos^2\theta^*}\right) \Big/ \left[\left(1+\frac{2\mathrm{M}^2_{\mathrm{e}^*}}{\mathrm{s}}\right)^2 - \cos^2\theta^*\right]. \tag{5}$$

Deviations from the QED $e^+e^- \to \gamma\gamma$ cross-section due to s-channel exchange of virtual gravitons were also probed. These can be parameterized as a function of $\frac{\lambda}{\mathrm{M}^4_{\mathrm{s}}}$, where $\mathrm{M_s}$ is the string mass scale, which in some string models could be of the order of the electroweak scale [18,19]. λ is a parameter entering Quantum Gravity models, conventionally taken to be $\pm$ 1. The ratio $\frac{\lambda}{\mathrm{M}^4_{\mathrm{s}}}$ follows the notation of [20] and is related to the Quantum Gravity scale, Λ_{T}, in reference [18] via:

$$\frac{|\lambda|}{\mathrm{M}^4_{\mathrm{s}}} = \frac{\pi}{2}\frac{1}{\Lambda^4_{\mathrm{T}}} \ \ [\mathrm{GeV}^{-4}]. \tag{6}$$

The 95% C.L. limits were extracted for the free parameters in these models. This was achieved using a binned maximum likelihood function, by renormalizing the joint probability to the physical region of each parameter according to the Bayesian approach described in [21]. The cross-section parameterization for the models considered, the chosen estimators (ξ) and the results of the likelihood function maximization are displayed in table 6 along with the 95% C.L. lower limits on each model parameter, Λ, $\mathrm{M}^*_{\mathrm{e}}$ and $\mathrm{M_s}$. The changes in the differential cross-section resulting from the range of fitted parameters are indicated by the dotted lines in figure 4. The final results presented in table 6 and in figure 4 were obtained by combining the results of the present analysis with results published previously [5]. The latter are based on LEP I data taken between 1990 and 1992, and on LEP II data collected between 1995 and 1997. Their centre-of-mass energies range from 91.2 GeV up to 182.7 GeV, corresponding to an integrated luminosity of 115.1 pb^{-1}.

5 Summary

The reaction $e^+e^- \to \gamma\gamma(\gamma)$ was studied using the LEP 1998 and 1999 high energy data, collected with the DELPHI detector at centre-of-mass energies of 188.6 GeV, 191.6

GeV, 195.5 GeV, 199.5 GeV and 201.6 GeV, corresponding to integrated luminosities of 151.9 pb^{-1}, 25.1 pb^{-1}, 76.1 pb^{-1}, 82.6 pb^{-1} and 40.1 $pb^{-}1$ respectively. The differential and total cross-sections for the process $e^+e^- \to \gamma\gamma$ were measured. Good agreement between the data and the QED prediction for this process was found. Lower limits on possible deviations from QED were derived by combining the present analysis result with a previously published one [5]. The 95% C.L. lower limits on the QED cut-off parameters of $\Lambda_+ >$330 GeV and $\Lambda_- >$ 320 GeV were obtained. In the framework of composite models, a 95% C.L. lower limit for the mass of an excited electron, $M_{e^*} > 311$ GeV/c^2, was obtained considering an effective coupling value of 1 for λ_γ. The possible contribution of virtual gravitons to the process $e^+e^- \to \gamma\gamma$ was probed, resulting in 95% C.L. lower limits in the string mass scale of $M_S > 713\,\mathrm{GeV/c^2}$ and $M_S > 691\,\mathrm{GeV/c^2}$ for $\lambda = 1$ and $\lambda = -1$ respectively (where λ is a $\mathcal{O}(1)$ parameter of Quantum Gravity models).

Acknowledgements

We are greatly indebted to our technical collaborators, to the members of the CERN-SL Division for the excellent performance of the LEP collider, and to the funding agencies for their support in building and operating the DELPHI detector.
We acknowledge in particular the support of
Austrian Federal Ministry of Science and Traffics, GZ 616.364/2-III/2a/98,
FNRS–FWO, Belgium,
FINEP, CNPq, CAPES, FUJB and FAPERJ, Brazil,
Czech Ministry of Industry and Trade, GA CR 202/96/0450 and GA AVCR A1010521,
Danish Natural Research Council,
Commission of the European Communities (DG XII),
Direction des Sciences de la Matière, CEA, France,
Bundesministerium für Bildung, Wissenschaft, Forschung und Technologie, Germany,
General Secretariat for Research and Technology, Greece,
National Science Foundation (NWO) and Foundation for Research on Matter (FOM), The Netherlands,
Norwegian Research Council,
State Committee for Scientific Research, Poland, 2P03B06015, 2P03B03311 and SPUB/P03/178/98,
JNICT–Junta Nacional de Investigação Científica e Tecnológica, Portugal,
Vedecka grantova agentura MS SR, Slovakia, Nr. 95/5195/134,
Ministry of Science and Technology of the Republic of Slovenia,
CICYT, Spain, AEN96–1661 and AEN96-1681,
The Swedish Natural Science Research Council,
Particle Physics and Astronomy Research Council, UK,
Department of Energy, USA, DE–FG02–94ER40817.

References

[1] F.A.Berends and R.Kleiss, *Nucl. Phys.* **B186** (1981) 22
[2] M.Böhm and T.Sack, Z.Phys.C **33** (1986) 157
[3] J.Fujimoto,M.Igarashi and Y.Shimizu, *Prog.of Theoretical Physics* **77** (1987) 118
[4] DELPHI Coll, P.Abreu et al., Phys. Lett. B**327**, 1994 (386)
[5] DELPHI Coll., P. Abreu et al., Phys. Lett. B**433**, 1998 (429)

[6] ALEPH Coll., Phys. Lett. B**429**, 1998 (201)
[7] L3 Coll., M. Acciari et al., Phys. Lett. B**475**, 2000 (198)
[8] OPAL Coll., G. Abbiendi et al., Phys. Lett. B**465**, 1999 (303)
[9] The LEP energy working group,
"Evaluation of the LEP centre-of-mass energy for data taken in 1998",
LEP Energy Group 99-01, March 1999
[10] DELPHI Coll., P.Abreu et al., *Nucl. Instrum. Methods* **A378** (1996) 57
[11] S.Jadach,W.Placzek and B.F.L.Ward, UTHEP-95-1001
[12] D.Karlen, *Nucl. Phys.* **B289** (1987) 23
[13] S.Catani et al., Phys. Lett. B**269**, 1991 (432)
[14] DELPHI Coll., P. Abreu et al., CERN-EP/2000-068
[15] S.Drell, *Ann.Phys.(NY)* **4**(1958)75
[16] F.E.Low, *Phys. Rev. Lett.* (1965) 238
[17] A.Blondel et al., CERN-EP/87-050 - ECFA/87-108 414
[18] G.F.Giudice, R.Rattazzi and J.D.Wells, *Nucl. Phys.* **B544** (1999) 3
[19] K.Agashe and N.G.Deshpande, Phys. Lett. B**456**, 1999 (60)
[20] J.L.Hewett, *Phys. Rev. Lett.* (1999) 4765
[21] Particle Data Group, *E.Phys.J.* **C3** (1998) 1

$\sqrt{s}$ [GeV]	$\epsilon^{\gamma\gamma}_{trigger}$	
	Barrel $\lvert\cos\theta^*\rvert \in [0.035, 0.731]$	Forward $\lvert\cos\theta^*\rvert \in [0.819, 0.906]$
188.6	0.985 ± 0.002	1.0000 ± 0.0003
191.6	0.977 ± 0.007	1.000 ± 0.002
195.5	0.977 ± 0.004	0.9995 ± 0.0005
199.5	0.968 ± 0.005	0.9995 ± 0.0005
201.6	0.983 ± 0.005	1.000 ± 0.001

Table 1: Trigger efficiencies (using the redundancy of the Bhabha trigger) for $\gamma\gamma$ neutral final states in the barrel and forward regions of the detector for the different data sets.

$\sqrt{s}$ [GeV]	$\epsilon^{\gamma\gamma+\gamma\gamma_c}_{sel}$	
	Barrel $\lvert\cos\theta^*\rvert \in [0.035, 0.731]$	Forward $\lvert\cos\theta^*\rvert \in [0.819, 0.906]$
188.6	$0.754 \pm 0.004 \pm 0.032$	$0.480 \pm 0.006 \pm 0.003$
191.6 - 201.6	$0.756 \pm 0.004 \pm 0.029$	$0.557 \pm 0.007 \pm 0.012$

Table 2: Selection efficiencies for $\gamma\gamma(\gamma)$ final states in the barrel and forward regions of the detector, with their statistical and systematic uncertainties, for the two data taking periods.

$\sqrt{s}$ = 188.6 GeV	$\lvert\cos\theta^*\rvert$	$N_{dat}^{\gamma\gamma+\gamma\gamma_c}$	($N_{QED} \pm \Delta N_{stat}$)	$N_{dat}^{\gamma\gamma_c}$	(N_{QED})	$d\sigma_{dat}^0/d\Omega$ [pb/str]
	0.035-0.136	46	(41.5 ± 1.4)	5	(6.2)	0.65 ± 0.10 ± 0.05
	0.136-0.237	48	(47.9 ± 1.5)	3	(3.8)	0.62 ± 0.09 ± 0.01
	0.237-0.338	64	(52.6 ± 1.6)	5	(6.4)	0.84 ± 0.11 ± 0.04
	0.338-0.439	57	(54.8 ± 1.5)	5	(6.2)	0.81 ± 0.11 ± 0.03
	0.439-0.540	77	(71.1 ± 1.8)	11	(8.5)	0.97 ± 0.11 ± 0.03
	0.540-0.641	76	(90.0 ± 2.0)	19	(10.8)	1.01 ± 0.12 ± 0.04
	0.641-0.731	108	(111.7 ± 2.3)	11	(15.8)	1.59 ± 0.15 ± 0.04
	0.819-0.906	176	(170.3 ± 2.8)	47	(53.4)	4.27 ± 0.32 ± 0.06
	total	652	(639.7 ± 5.4)	106	(111.1)	

$\sqrt{s}$ = 191.6 GeV	$\lvert\cos\theta^*\rvert$	$N_{dat}^{\gamma\gamma+\gamma\gamma_c}$	($N_{QED} \pm \Delta N_{stat}$)	$N_{dat}^{\gamma\gamma_c}$	(N_{QED})	$d\sigma_{dat}^0/d\Omega$ [pb/str]
	0.035-0.136	6	(6.4±0.3)	2	(0.9)	0.53 ± 0.22 ± 0.09
	0.136-0.237	6	(7.2±0.3)	0	(0.7)	0.52 ± 0.21 ± 0.05
	0.237-0.338	8	(8.5±0.3)	1	(0.9)	0.62 ± 0.22 ± 0.04
	0.338-0.439	6	(9.9±0.3)	1	(1.1)	0.48 ± 0.20 ± 0.03
	0.439-0.540	10	(12.4±0.4)	1	(1.5)	0.79 ± 0.25 ± 0.05
	0.540-0.641	14	(14.7±0.4)	5	(1.8)	1.09 ± 0.29 ± 0.09
	0.641-0.731	13	(17.8±0.4)	1	(2.7)	1.17 ± 0.32 ± 0.03
	0.819-0.906	27	(31.3±0.6)	8	(7.7)	3.42 ± 0.66 ± 0.09
	total	90	(108.2±1.1)	19	(17.3)	

$\sqrt{s}$ = 195.5 GeV	$\lvert\cos\theta^*\rvert$	$N_{dat}^{\gamma\gamma+\gamma\gamma_c}$	($N_{QED} \pm \Delta N_{stat}$)	$N_{dat}^{\gamma\gamma_c}$	(N_{QED})	$d\sigma_{dat}^0/d\Omega$ [pb/str]
	0.035-0.136	21	(19.3±0.8)	4	(2.5)	0.61 ± 0.13 ± 0.03
	0.136-0.237	29	(21.5±0.8)	5	(2.1)	0.80 ± 0.15 ± 0.04
	0.237-0.338	9	(24.6±0.9)	0	(2.5)	0.23 ± 0.08 ± 0.01
	0.338-0.439	23	(27.4±0.9)	4	(3.2)	0.64 ± 0.13 ± 0.02
	0.439-0.540	48	(36.6±1.1)	2	(4.4)	1.23 ± 0.18 ± 0.03
	0.540-0.641	47	(43.2±1.2)	6	(5.3)	1.21 ± 0.18 ± 0.06
	0.641-0.731	58	(51.7±1.7)	12	(7.9)	1.72 ± 0.23 ± 0.04
	0.819-0.906	102	(91.0±1.7)	28	(22.6)	4.29 ± 0.42 ± 0.08
	total	337	(315.3 ± 3.1)	61	(50.5)	

$\sqrt{s}$ = 199.5 GeV	$\lvert\cos\theta^*\rvert$	$N_{dat}^{\gamma\gamma+\gamma\gamma_c}$	($N_{QED} \pm \Delta N_{stat}$)	$N_{dat}^{\gamma\gamma_c}$	(N_{QED})	$d\sigma_{dat}^0/d\Omega$ [pb/str]
	0.035-0.136	19	(21.2±0.8)	3	(2.5)	0.51 ± 0.12 ± 0.03
	0.136-0.237	17	(23.0±0.9)	0	(2.5)	0.42 ± 0.10 ± 0.03
	0.237-0.338	28	(23.7±0.9)	2	(2.4)	0.70 ± 0.13 ± 0.04
	0.338-0.439	34	(25.0±0.9)	3	(3.7)	0.93 ± 0.16 ± 0.05
	0.439-0.540	39	(35.2±1.1)	1	(4.5)	0.91 ± 0.15 ± 0.03
	0.540-0.641	45	(45.4±1.2)	4	(6.3)	1.11 ± 0.16 ± 0.05
	0.641-0.731	40	(54.9±1.4)	9	(6.8)	1.07 ± 0.17 ± 0.03
	0.819-0.906	88	(96.0±1.8)	29	(24.4)	3.37 ± 0.36 ± 0.09
	total	310	(324.3±3.3)	51	(53.1)	

$\sqrt{s}$ = 201.6 GeV	$\lvert\cos\theta^*\rvert$	$N_{dat}^{\gamma\gamma+\gamma\gamma_c}$	($N_{QED} \pm \Delta N_{stat}$)	$N_{dat}^{\gamma\gamma_c}$	(N_{QED})	$d\sigma_{dat}^0/d\Omega$ [pb/str]
	0.035-0.136	14	(10.7±0.4)	2	(1.2)	0.72 ± 0.19 ± 0.06
	0.136-0.237	8	(10.9±0.4)	0	(1.2)	0.40 ± 0.14 ± 0.04
	0.237-0.338	17	(11.7±0.4)	4	(1.2)	0.84 ± 0.20 ± 0.08
	0.338-0.439	12	(13.3±0.5)	1	(1.8)	0.60 ± 0.17 ± 0.03
	0.439-0.540	13	(16.6±0.5)	0	(2.1)	0.63 ± 0.17 ± 0.03
	0.540-0.641	21	(21.7±0.6)	1	(3.0)	1.06 ± 0.23 ± 0.04
	0.641-0.731	19	(26.1±0.6)	4	(3.2)	1.05 ± 0.24 ± 0.03
	0.819-0.906	43	(45.6±0.9)	15	(11.6)	3.39 ± 0.52 ± 0.10
	total	147	(156.6±1.6)	27	(25.3)	

Table 3: Number of events selected from data as a function of $|\cos\theta^*|$ and number of expected events (in parenthesis) from QED corrected for trigger efficiency. The uncertainties associated to the QED predictions are statistical only. In the third column the number of events with one converted photon is given along with the QED simulation prediction. In the fourth column the measured Born differential cross-section is displayed

$\sqrt{s}$	analysis acceptance		$\cos\theta^* \in [-0.742, 0.742]$	
[GeV]	σ^0_{dat} [pb]	σ^0_{QED} [pb]	σ^0_{dat} [pb]	σ^0_{QED} [pb]
188.6	6.34 ± 0.25 ± 0.16	6.27	4.27 ± 0.20 ± 0.14	4.28
191.6	5.09 ± 0.54 ± 0.13	6.08	3.43 ± 0.43 ± 0.11	4.15
195.5	6.31 ± 0.34 ± 0.13	5.83	4.22 ± 0.28 ± 0.09	3.98
199.5	5.34 ± 0.30 ± 0.17	5.60	3.73 ± 0.25 ± 0.14	3.82
201.6	5.14 ± 0.42 ± 0.16	5.49	3.50 ± 0.34 ± 0.13	3.74
193.8	5.89 ± 0.15 ± 0.16	5.94	4.00 ± 0.12 ± 0.12	4.05

Table 4: Measured Born cross-sections for $e^+e^- \to \gamma\gamma$ (with statistical and systematic uncertainties) at the different centre-of-mass energies, for the analysis $\cos\theta^*$ acceptance and for the barrel region ($42^\circ < \theta^* < 138^\circ$), compared to the corresponding QED predictions. In the last line the combined results are displayed along with the QED cross-sections at a centre-of-mass energy of 193.8 GeV.

$\lvert\cos\theta^*\rvert$	$\mathrm{d}\sigma^0_{\mathrm{dat}}/\mathrm{d}\Omega$ [pb/str]	$\mathrm{d}\sigma^0_{\mathrm{QED}}/\mathrm{d}\Omega$ [pb/str]
0.035-0.136	0.61 ± 0.06± 0.04	0.56
0.136-0.237	0.58 ± 0.06± 0.03	0.59
0.237-0.338	0.67 ± 0.06± 0.03	0.65
0.338-0.439	0.75 ± 0.07± 0.03	0.75
0.439-0.540	0.96 ± 0.07± 0.03	0.90
0.540-0.641	1.08 ± 0.08± 0.04	1.14
0.641-0.731	1.41 ± 0.09± 0.03	1.53
0.819-0.906	3.90 ± 0.19± 0.08	3.76

Table 5: Measured and predicted Born differential cross-section (the measured cross-section uncertainties are statistical and systematic) for the QED process $e^+e^- \to \gamma\gamma$ at a mean centre-of-mass energy of 193.8 GeV obtained by combining the data sets corresponding to centre-of-mass energies of 189.6 GeV, 191.6 GeV, 195.5 GeV, 199.5 GeV and 201.6 GeV.

	Cut-off		Composite	Low M_s	
$(\frac{d\sigma}{d\Omega})^D$	$\frac{\alpha^2 s}{2}(1+\cos^2\theta^*)\cdot\xi$		$\frac{\alpha^2 s}{2}(1+\cos^2\theta^*)H(\cos^2\theta^*)\cdot\xi$	$\frac{\alpha s}{4\pi}(1+\cos^2\theta^*)\cdot\xi+\mathcal{O}(\xi^2)$	
ξ	$\pm 1/\Lambda_{\pm}^4$		$(\lambda_\gamma/M_{e^*}^2)^2$	λ/M_s^4	
$\xi^{+\sigma_+}_{-\sigma_-}$ (1998-1999)	$(0.034^{+0.547}_{-0.530})10^{-10}$		$(0.048^{+0.679}_{-0.611})10^{-10}$	$(0.015^{+0.251}_{-0.243})10^{-11}$	
$\xi^{+\sigma_+}_{-\sigma_-}$ (1990-1999)	$(-0.131^{+0.515}_{-0.501})10^{-10}$		$(-0.176^{+0.654}_{-0.599})10^{-10}$	$(-0.060^{+0.236}_{-0.230})10^{-11}$	
95% C.L. lower limits	Λ_+ [GeV]	Λ_- [GeV]	M_{e^*} [GeV/c^2] $\lambda_\gamma = 1$	M_s [GeV/c^2] $\lambda = +1$	M_s [GeV/c^2] $\lambda = -1$
	330	320	311	713	691

Table 6: Parameterization for each model predicting a deviation from QED, chosen estimator (ξ), output of the likelihood function maximization for the results of the present analysis and for their combination with those previously published [4], resulting in 95% C.L. lower limits on each model parameter. Both in the case of the excited electron and of the string mass scale, the values given for ξ correspond to setting λ_γ and $|\lambda|$ to 1.

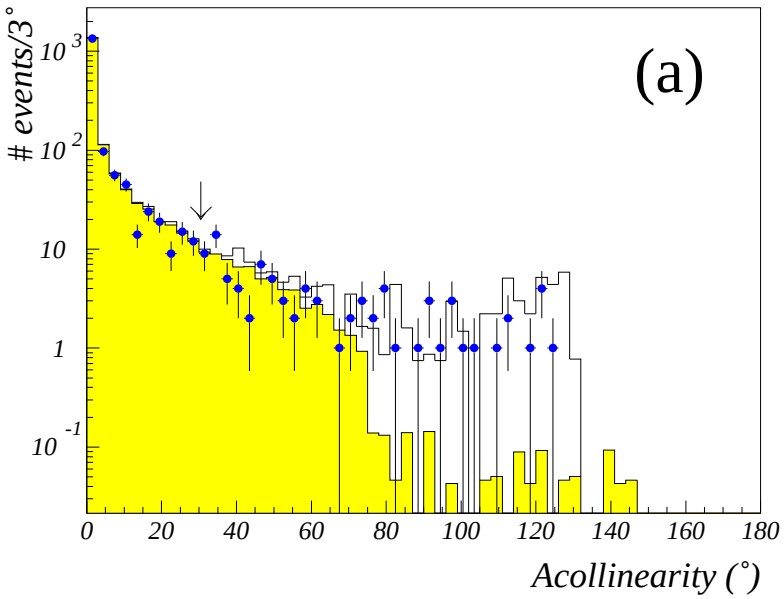

Figure 1: Acollinearity distribution for the $\gamma\gamma(\gamma)$ sample selected at all centre-of-mass energies (dots), before imposing the 30° acollinearity cut (arrow). The histograms represent the QED $e^+e^- \to \gamma\gamma(\gamma)$ simulation (grey area) and the remaining background (white area). The latter is mainly due to Compton ($e^{\pm}\gamma$) events.

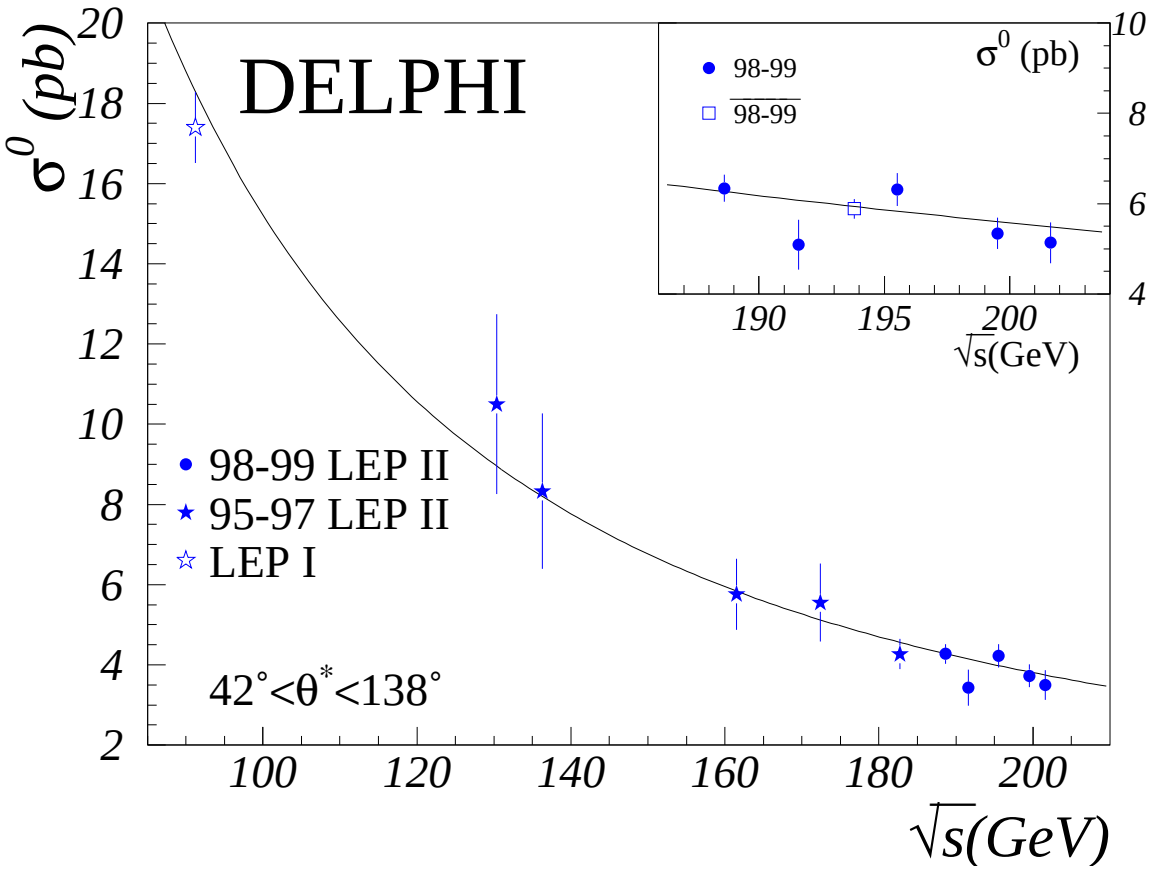

Figure 2: Born cross-section for $e^+e^- \to \gamma\gamma$ in the barrel region of DELPHI, $42^\circ < \theta^* < 138^\circ$, as a function of the centre-of-mass energy, for 1990-1992 LEP I data (white star), LEP II data collected between 1995 and 1997 (black stars), and for the data collected during 1998 and 1999 (dots), compared to the QED prediction. The Born cross-section measured within the analysis acceptance region for the real data collected during 1998 and 1999 (dots) and the cross-section resulting from the combination of these data sets at an average centre-of-mass energy of 193.8 GeV (square) are compared to the QED prediction in the upper right plot.

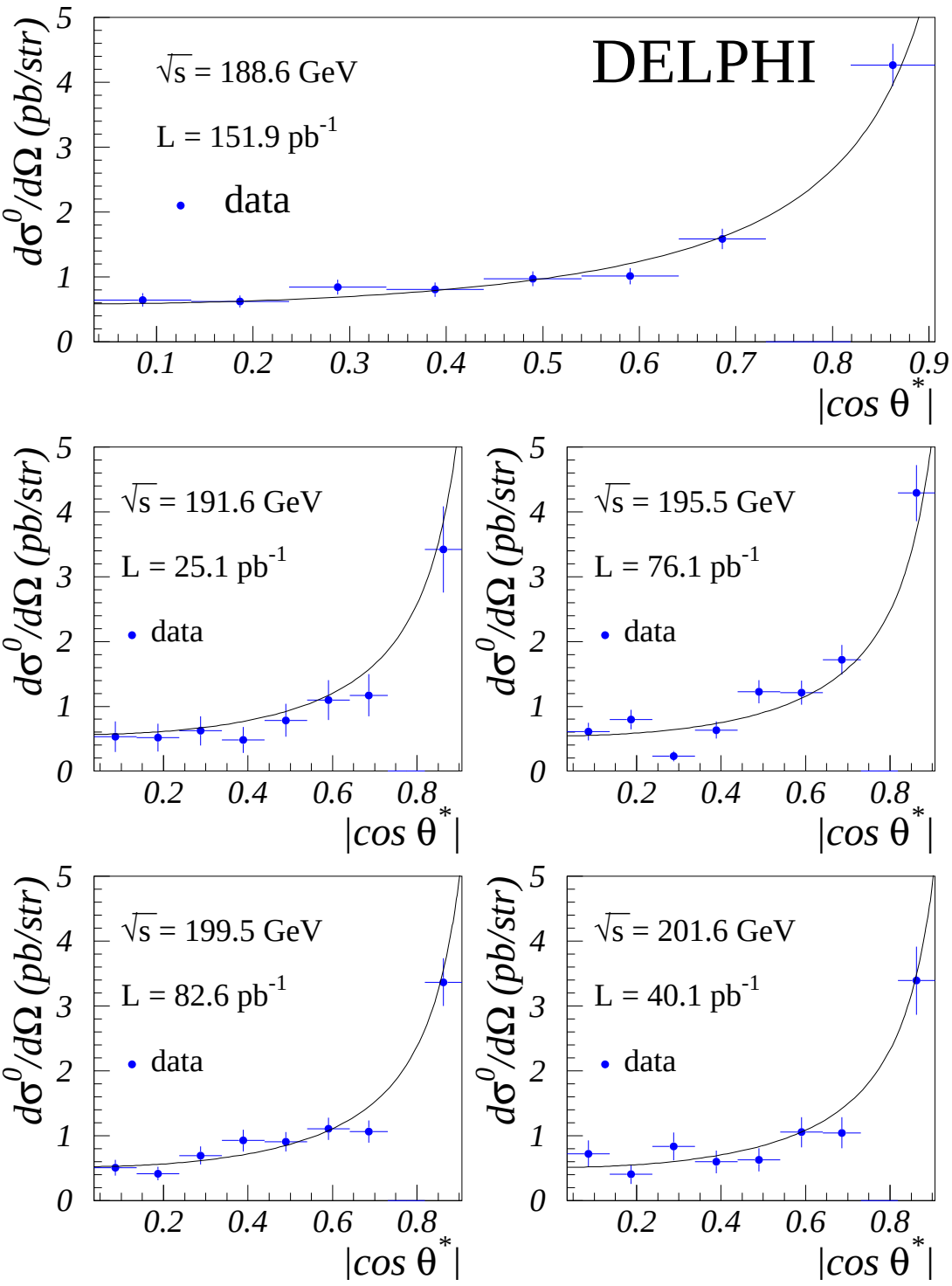

Figure 3: Differential Born cross-section distributions obtained for the five centre-of-mass energies compared to the corresponding QED theoretical predictions.

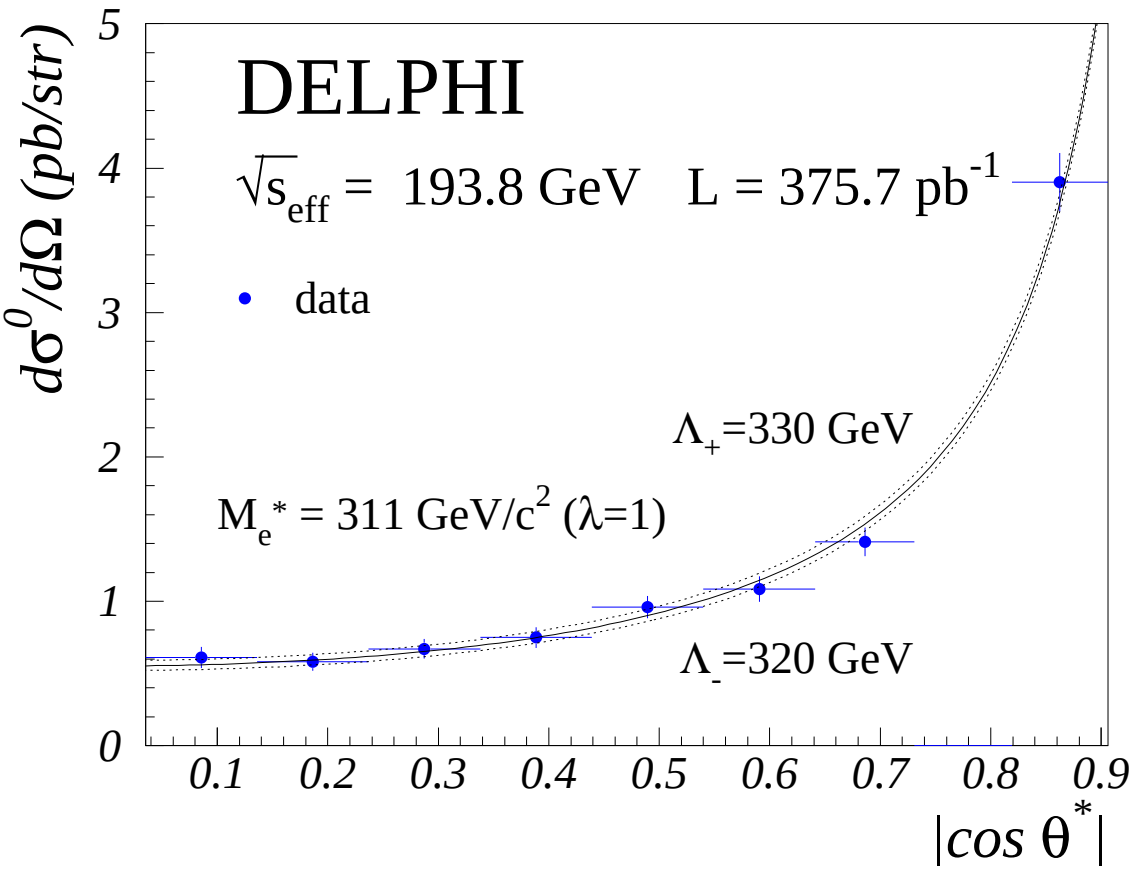

Figure 4: Born differential cross-section obtained by combining all data sets at an effective centre-of-mass energy of 193.8 GeV (dots), compared to the QED theoretical distribution (full line). The dotted lines represent the allowed 95% C.L. deviations from the QED differential cross-section, which correspond to 95% C.L. lower limits on Λ_+ and Λ_- of 330 GeV and 320 GeV respectively, to a 311 GeV/c^2 95% C.L. lower limit on the excited electron mass (for $\lambda_\gamma = 1$), and to 95% C.L. lower limits on the string mass scale of 713 GeV/c^2 (for $\lambda = 1$) and 691 GeV/c^2 (for $\lambda = -1$).